International Geology Review
Publication details, including instructions for authors and subscription information:
http://www.tandfonline.com/loi/tigr20

Origin of early Triassic rift-related alkaline basalts from Southwest China: age, isotope, and trace-element constraints

Jiawei Zhang [a b], Zhilong Huang [a], Taiyi Luo [a], Zhikuan Qian [a b] & Ying Zhang [a b]

[a] State Key Laboratory of Ore Deposit Geochemistry, Institute of Geochemistry, Chinese Academy of Sciences, Guiyang, 550002, China

[b] University of Chinese Academy of Sciences, Beijing, 100049, China

Published online: 14 Feb 2013.

To cite this article: Jiawei Zhang, Zhilong Huang, Taiyi Luo, Zhikuan Qian & Ying Zhang (2013) Origin of early Triassic rift-related alkaline basalts from Southwest China: age, isotope, and trace-element constraints, International Geology Review, 55:9, 1162-1178, DOI: 10.1080/00206814.2013.767526

To link to this article: http://dx.doi.org/10.1080/00206814.2013.767526

International Geology Review, 2013
Vol. 55, No. 9, 1162–1178, http://dx.doi.org/10.1080/00206814.2013.767526

Taylor & Francis
Taylor & Francis Group

Origin of early Triassic rift-related alkaline basalts from Southwest China: age, isotope, and trace-element constraints

Jiawei Zhang[a,b], Zhilong Huang[a]*, Taiyi Luo[a], Zhikuan Qian[a,b] and Ying Zhang[a,b]

[a]*State Key Laboratory of Ore Deposit Geochemistry, Institute of Geochemistry, Chinese Academy of Sciences, Guiyang 550002, China;* [b]*University of Chinese Academy of Sciences, Beijing 100049, China*

(*Accepted 23 December 2012*)

We report new analytical data regarding major and trace element geochemistry, Sr-Nd isotopic composition, and zircon LA-ICP-MS U-Pb analysis from the Kaiyuan alkaline basalts of Yunnan Province, along the southern margin of the Emeishan Large Igneous Province (ELIP). Zircon U-Pb ages and bulk-rock geochemistry indicate that the mafic lavas erupted at 248 ± 6 Ma with OIB-like trace element and isotope ratios similar to the Emeishan high-Ti basalts. These characters suggest that the Kaiyuan alkaline basalts are the products of the post-ELIP magmatism, involving remelting of the plume head after the main ELIP phase. By analogy with the Neogene Red Sea rift system, the Kaiyuan alkaline basalts may have been caused by a Red Sea-like extension along the southwestern margin of the Yangzte during the Early Triassic, during which the hypothesized rift system experienced plate–boundary forces that vanished quickly in the Late Triassic period.

Keywords: alkaline basalt; rift system; Kaiyuan alkali basalt petrogenesis; Emeishan large igneous province; Southwest China

Introduction

The Emeishan continental flood basalts (ECFB), covering an area of over 5×10^5 km^2 in southwest China and northern Vietnam, have been studied extensively over the last decade (Xu *et al.* 2001; Zhou *et al.* 2002; Xu *et al.* 2004; Ali *et al.* 2005; Song *et al.* 2008; Zhou *et al.* 2008; Ali *et al.* 2010; Hanski *et al.* 2010; Shellnutt and Jahn 2010, 2011; Zhong *et al.* 2011). However, the origin of the Kaiyuan Anisian basalts in the southern part of the ELIP (Figure 1A) is poorly understood. A detailed investigation of the geochemical characters of these rocks could provide useful information about their origin and petrogensis. In addition to the Kaiyuan district, the Anisian basaltic lavas, which are present in the Gejiu formation (T_2g), were also discovered in the Gejiu and Funing areas (YBGMR 1982; Xue 2002). The study of Kaiyuan alkaline basalts is critically important because it represents an important petrological comparative subject for other Anisian basalts.

The transverse tectonic structures of the Afar Depression are characterized by alkaline basaltic volcanism, which contrasts with the transitional basaltic volcanism of the axial ranges (Teklay *et al.* 2010 and references therein). Accordingly, a comparison with the well-known Red Sea rift system and coeval volcanism may provide useful information to understand the history of the other plume-rift systems.

In this study, we report major- and trace-element geochemistry, Sr-Nd isotopic compositions, and LA-ICP-MS zircon U-Pb analysis of the Kaiyuan alkaline basalts. By contrasting the tectonic structure and correlative magmatism events of the Red Sea rift area; our new analytical data from Southwest China indicate that although the geochemical features are similar to the ECFB, the Kaiyuan alkaline basalts are the products of post-ELIP magmatism at 248 Ma. This activity was caused by a Red Sea-like rift extension after the main phase of ELIP along the SW margin of the Yangzte craton.

Field geology and petrography

The Kaiyuan alkaline basalts are located at the southern part of the ELIP (Figure 1A) and outcrop on the eastern part of the Dongliancun, Kaiyuan city (Figure 1B).

The Middle Triassic Gejiu formation (T_2g) and Falang formation (T_2f) and the Late Triassic Niaoge formation (T_3n) are the dominant strata. The Gejiu formation comprises mainly carbonates. The Falang formation is composed of sandstones and shales and the Niaoge formation is made up of aleurolite (YBGMR 1982).

*Corresponding author. Email: huangzhilong@vip.gyig.ac.cn

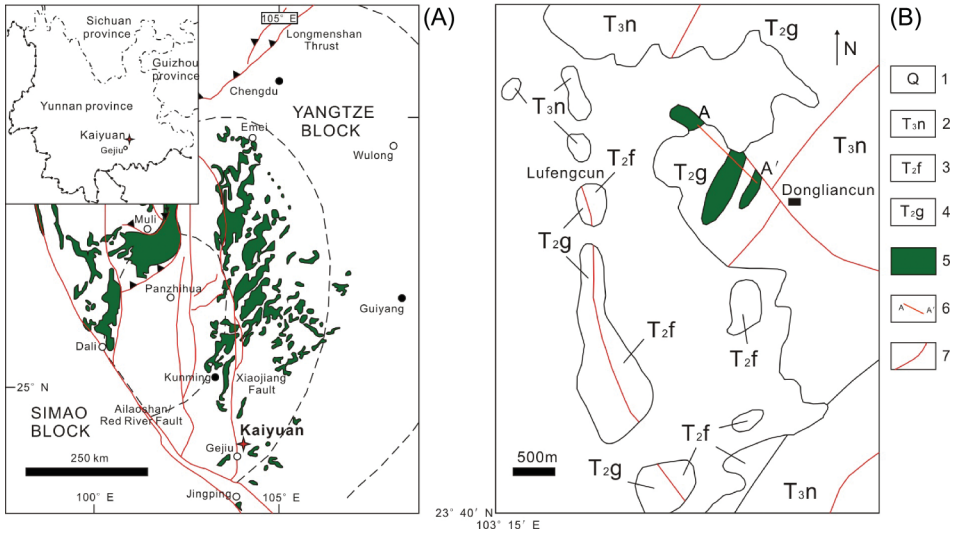

Figure 1. (A) Simplified map showing the Emeishan basalt outcrop. Dashed curves separate inner, intermediate, and outer zones of the dome, which are characterized by varying extents of erosion of Maokou limestone. Based on Xu *et al.* (2004) and Ali *et al.* (2005); (B) Geolocal map of Kaiyuan area. 1–Quaternary; 2–Triassic niaoge formation; 3–Triassic feixianguan formation; 4–Triassic gejiu fomation; 5–outcrop of Kaiyuan alkaline basalts; 6–measured section; 7–fault.

One profile cut across these three units is selected to study the characters of the Kaiyuan alkaline basalts. The profile is 1265 m long, with a striking angle of 135°, which starts at A (23° 43′ 20.5″ N, 103° 16′ 40.4″ E) and ends at A' (23° 42′ 51.7″ N, 103° 17′ 12.4″ E).

According to the petrographic characteristics, the Kaiyuan alkaline basalts are divided into three units with intercalated sedimentary rocks. The upper unit is composed of dark brown and dark green pillow structure basalts. The dark red basaltic andesite is found at the borderline between the upper and middle unit. The dark brown massive structure basalts and the carbonate rocks alternately occur in the middle unit. The lower unit consists of dark brown basalts with amygdaloidal structure. The amygdaloids are filled with calcites. Details of the petrography and sampling are shown in Figure 2.

Analytical procedures

Zircon LA-ICP-MS U-Pb dating

The KYB sample was selected for chronological study. For cathodoluminescent (CL) imaging, representative zircon grains were handpicked and mounted in epoxy resin discs and subsequently polished and coated with carbon. The internal morphology was examined using CL prior to U-Pb isotopic analysis. Laser ablation ICP-MS and zircon U-Pb analysis were performed on an Agilent 7500a ICP-MS equipped with a 193 nm laser, which was housed at the State Key Laboratory of Continental Dynamics, Northwest University in Xi'an, China. A zircon 91500 was used as an external standard to normalize isotopic fractionation during the isotope analysis. NIST610 glass was used as an external standard to normalize the U, Th and Pb concentrations of the unknowns. The diameter of each spot was 30 μm. Details of the analytical technique were given in Zong *et al.* (2010). The common Pb contents were evaluated using the method described by Andersen (2002). The age computations and concordia diagrams were made using ISOPLOT (version 3.0) (Ludwig 2003). The errors quoted in the tables and figures were at the 1σ level, and the weighted average ages were calculated at the 2σ level.

The zircon trace element analyses were simultaneously obtained during zircon U-Pb dating. NIST610 was used as an external standard to calculate the trace element contents of the unknowns. A detailed compilation of the instrument and data acquisition parameters is presented in Liu *et al.* (2010).

Whole-rock major and trace element analysis

A detailed petrographic examination was carried out on the studied samples to avoid the effects of secondary alteration and weathering, which were subsequently pulverized using an agate mill.

Twelve samples were chosen for the whole-rock major and trace element analysis in the Mineral-Chemex Division of ALS Laboratory Group (Guangzhou, China). The calcined or ignited sample for major element analysis (0.9 g) was added to 9.0 g of Lithium Borate Flux (50–50% $Li_2B_4O_7$-$LiBO_2$), mixed well and fused in an auto fluxer between 1050 and 1100°C. A flat molten glass disc was prepared from the resulting melt. This disc was then analysed by X-ray fluorescence spectrometry. The relative standard deviation (RSD) and relative error (RE) were better than 2%.

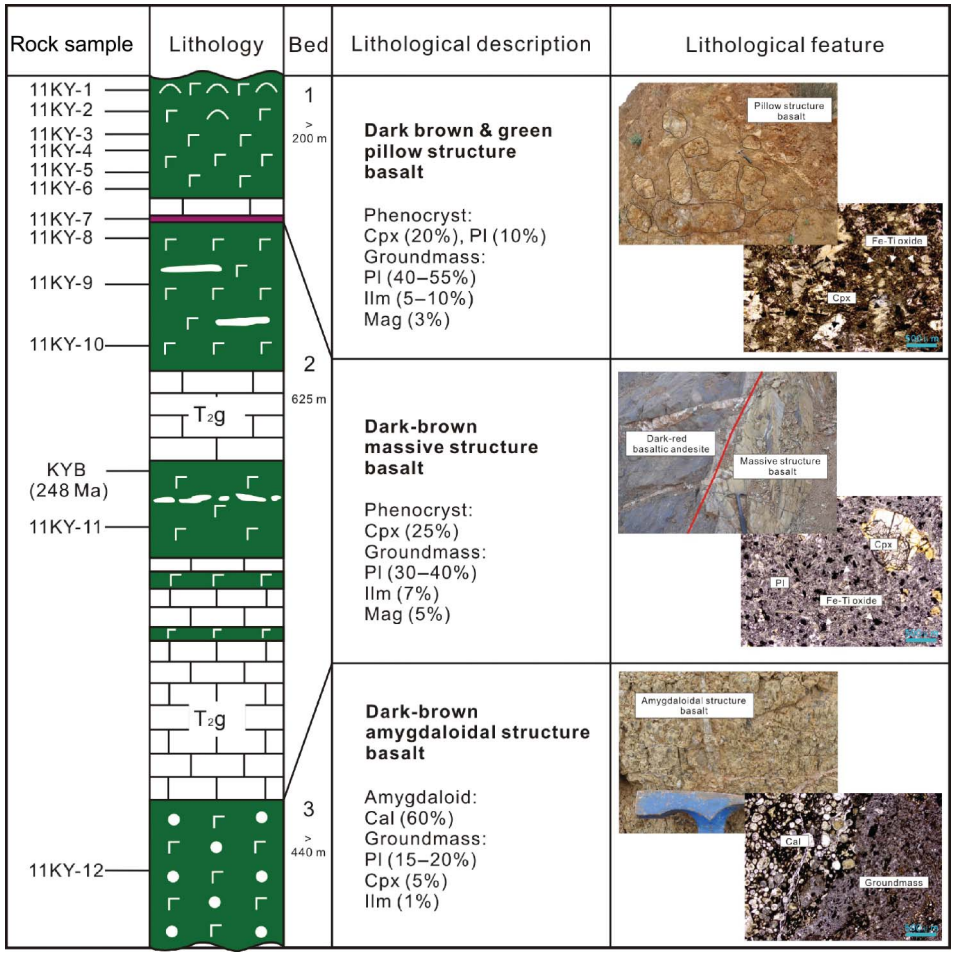

Figure 2. Composite stratigraphic column of the Kaiyuan basalt measured section.

In terms of the trace-element analytical process, the prepared sample was added to lithium metaborate flux, mixed well, and fused in a furnace at 1000°C. The resulting melt was then cooled and dissolved in 100 ml of 4% HNO_3/2% HCl solution. This solution was analysed by inductively coupled plasma mass spectrometry. The relative standard deviation (RSD) and relative error (RE) was less than 5%.

Analysis of Rb-Sr and Sm-Nd radiogenic isotope ratios

The Rb-Sr and Sm-Nd isotopic measurements were performed on the MAT-262 TIMS at the Institute of Geochemistry, Chinese Academy of Sciences (IGCAS), Guiyang. The chemical separation and isotopic measurement procedures followed Zhang *et al.* (2001). The mass fractionation corrections for the Sr and Nd isotopic ratios were based on $^{86}Sr/^{88}Sr = 0.1194$ and $^{146}Nd/^{144}Nd = 0.7219$, respectively. The analyses of the standards during the period of analysis were as follows: NBS987 Sr standard yielded an $^{87}Sr/^{86}Sr = 0.710255 \pm 0.000007$ (2σ); JNdi-1 Nd standard yielded a $^{143}Nd/^{144}Nd = 0.512096 \pm 0.000005$ (2σ). The uncertainties in Rb-Sr and Sm-Nd ratios are less than ±2% and ±0.5% (relative).

Results

LA-ICP-MS zircon U-Pb dating

The LA-ICP-MS zircon U-Pb dating results are listed in Table 1, and the trace elements of zircons are in Table 2. Thirty analyses are made and nine results fall in a single population of 254–243 Ma. The measurements form a cluster on the concordia plot with a weighted mean $^{206}Pb/^{238}U$ age of 248.2 ± 6.1 Ma (MSWD = 0.25) (Figure 3B). Those nine zircons are 50–100 μm in size and show clear, pale, and euhedral appearances, with magmatic oscillatory zoning without inclusions, cores, and cracks evident in the CL images (Figure 4). The zircons possess a relatively wide range in the U (75.66–761.15 ppm) and Th (40.95–447.80 ppm) contents, with Th/U ratios ranging from 0.48 to 1.09 (Table 2) and displaying a strong linear array ($R^2 = 0.943$). The rare earth element (REE) patterns of each zircon (not shown) display similar trends.

Table 1. LA-ICP-MS analytical results of all zircons from Kaiyuan basalts.

	Calculated ratios						Ages (Ma)					
	$^{207}Pb/^{206}Pb$		$^{207}Pb/^{235}U$		$^{206}Pb/^{238}U$		$^{207}Pb/^{206}Pb$		$^{207}Pb/^{235}U$			
	Ratio	1 sigma	Ratio	1 sigma	Ratio	1 sigma	Age	2 sigma	Age	2 sigma	Age	2 sigma
Basalts zircons												
KYB-09	0.05638	0.00049	0.3051	0.00568	0.03916	0.00054	467	19	270	4	248	3
KYB-13	0.06168	0.00073	0.34127	0.00782	0.04009	0.00057	663	25	298	6	253	4
KYB-14	0.04798	0.00498	0.26154	0.03028	0.03954	0.00069	98	217	236	24	250	4
KYB-15	0.05047	0.00183	0.26723	0.01303	0.0384	0.00057	217	83	240	10	243	4
KYB-16	0.05953	0.00072	0.31856	0.00737	0.03879	0.00055	587	26	281	6	245	3
KYB-21	0.05077	0.00213	0.26692	0.01475	0.03813	0.00059	230	95	240	12	241	4
KYB-24	0.05456	0.00471	0.29907	0.03097	0.03976	0.00078	394	190	266	24	251	5
KYB-28	0.0525	0.0019	0.29121	0.01411	0.04023	0.0006	307	80	260	11	254	4
KYB-30	0.05908	0.00097	0.32726	0.00934	0.04019	0.0006	570	35	287	7	254	4
Inherited zircons												
KYB-01	0.06699	0.00063	0.44755	0.00883	0.04825	0.00067	837	19	376	6	304	4
KYB-02	0.06694	0.00054	1.29545	0.02285	0.13981	0.00191	836	16	844	10	844	11
KYB-03	0.15878	0.00315	0.57398	0.02021	0.02612	0.0005	2443	33	461	13	166	3
KYB-04	0.06528	0.00171	0.65239	0.02644	0.07223	0.00124	783	54	510	16	450	7
KYB-05	0.09745	0.00104	1.2804	0.02784	0.09498	0.00139	1576	19	837	12	585	8
KYB-06	0.11041	0.0007	4.94422	0.07108	0.32386	0.0044	1806	11	1810	12	1809	21
KYB-07	0.06208	0.00118	0.4149	0.0131	0.04834	0.00074	677	40	352	9	304	5
KYB-08	0.07857	0.0006	0.68181	0.01167	0.06278	0.00086	1161	15	528	7	393	5
KYB-10	0.11636	0.00251	0.33917	0.01219	0.0211	0.00037	1901	38	297	9	135	2
KYB-11	0.07563	0.00045	1.30295	0.01746	0.12478	0.00167	1085	12	847	8	758	10
KYB-12	0.13418	0.00108	7.1548	0.1343	0.38673	0.00539	2153	14	2131	17	2108	25
KYB-17	0.14591	0.00186	7.72623	0.19301	0.38405	0.00573	2298	22	2200	22	2095	27
KYB-18	0.15519	0.00238	0.96776	0.02781	0.04522	0.00077	2404	26	687	14	285	5
KYB-19	0.05716	0.00037	0.63143	0.0095	0.0801	0.00109	498	14	497	6	497	7
KYB-20	0.06934	0.00059	1.42307	0.02628	0.14884	0.00209	909	17	899	11	894	12
KYB-22	0.05038	0.00236	0.17287	0.01047	0.02488	0.0004	213	105	162	9	158	3
KYB-23	0.67381	0.00425	15.11326	0.21532	0.16273	0.00227	4676	9	2822	14	972	13
KYB-25	0.05877	0.00177	0.33967	0.01457	0.04191	0.00063	559	64	297	11	265	4
KYB-26	0.05817	0.00181	0.65085	0.02812	0.08115	0.0012	536	67	509	17	503	7
KYB-27	0.73067	0.00467	22.21192	0.32168	0.22058	0.00309	4792	9	3193	14	1285	16
KYB-29	0.05578	0.00082	0.50221	0.01316	0.0653	0.0009	443	32	413	9	408	5

Geochemistry of major and trace elements

Owing to the calcite amygdaloids in the lower unit of the basalts, it is difficult to evaluate the real composition. However, the sample 11KY-12 has high SiO_2 (33.51%) and TiO_2 contents (2.55%). The sample shares many high field strength elements (HSFE) and REE similarities with the basalts of the upper and middle unit, which indicates it is a basalt.

The geochemical differences between the upper and middle unit are undistinguishable (Table 3). The recalculated SiO_2 contents (recalculated to 100 wt.% on a volatile-free basis) of all the basalt samples are over 44 wt.% and the dark-red andesite (11KY-7) between the upper and middle units have SiO_2 content of 56 wt.%. All the basalt samples have TiO_2 contents greater than 3.2 wt.% (ranging from 3.22 to 3.72 wt.%), which are consistent with the previous identification of Emeishan high-Ti series basalts (Wang and Zhou 2007). In addition, all the basalt samples display variable contents of MgO (6.46–11.52 wt.%), Al_2O_3 (12.13–14.47 wt.%), Fe_2O_3 (11.20–16.06 wt.%), and CaO (3.19–10.34 wt.%). The major and trace element variation diagrams are illustrated in Figure 5 with the Mg number as the differentiation index. Most of the basalt samples (except 11KY-6) belong to the alkaline series basalt based on the total alkali–silica (TAS) diagram (Figure 6A), and all of the plots (including the strongly altered sample, 11KY-12) fall in the field of alkaline basalts in the Zr/Ti *versus* Nb/Y diagram (Figure 6B). The CIPW norm mineral calculation of Kaiyuan alkaline basalts are presented in Table 4. Only half of the samples (11KY-3; 11KY-4; 11KY-6; 11KY-8; and 11KY-11) are nepheline-normative, silica-undersaturated basalts. The other samples (11KY-1; 11KY-2; 11KY-5; 11KY-9; and 11KY-10) are olivine-hypersthene normative, silica-saturated basalts. Therefore, the Kaiyuan alkaline basalts are transitional in characteristics with respect to the CIPW norm mineral calculation.

In the primitive mantle-normalized diagram (Figure 7A), the basalts have patterns with enriched large ion lithophile elements (LILE) (Rb, Ba, and K),

Table 2. Trace elemets of selected zircons gains.

Sample	KYB-9	KYB-13	KYB-14	KYB-15	KYB-16	KYB-21	KYB-24	KYB-28	KYB-30
Ti	11.35	7.3	27.34	158.02	5.58	16.68	19.3	182.44	12.93
Y	3212	2165	494.5	1243	1150	986.3	1560	1079	1123
Nb	4.31	1.77	1.52	1.91	1.97	1.32	3.46	3.7	1.36
La	0.165	0.052	1.187	0.262	0.18	<0.024	0.025	0.995	0.054
Ce	28.53	5.39	3.64	14.26	38.31	2.32	38.13	14.02	2.45
Pr	0.436	0.269	0.253	0.269	0.211	0.112	0.238	0.555	0.088
Nd	5.51	4.56	1.41	2.98	3.36	2.38	3.83	4.4	1.48
Sm	10.98	9.29	1.6	4.35	5.88	4.45	7.03	5.39	3.9
Eu	1.065	1.17	0.149	1.014	1.74	0.213	3.66	0.55	0.198
Gd	61.11	51.33	9.33	20.39	27.44	22.74	36.12	24.78	23.05
Tb	24.57	18.42	3.56	7.73	9.34	8.1	12.37	8.78	8.81
Dy	300.51	213.86	43.6	95.66	105.7	94.3	143.29	103.2	104.17
Ho	116.38	79.27	17.57	39.92	39	35.37	54.88	38.67	40.02
Er	492.76	331.37	77.19	197.72	170.25	149.77	236.43	165.58	171.44
Tm	104.16	66.45	16.45	49.33	38.08	30.81	49.07	34.13	36
Yb	923.96	599.49	156.77	538.75	374.11	286.1	459.06	309.25	329.73
Lu	157.62	104.19	28.5	111.54	67.16	50.88	83.09	52.74	57.94
Ta	1.9	0.625	0.445	0.734	0.659	0.52	0.871	1.626	0.572
Pb^{204}	2.33	1.27	3.8	3.18	1.25	<0.86	<0.87	52.48	<0.86
Pb^{206}	121.5	55.23	16.94	96.46	48.75	25.74	12.51	158.77	26.66
Pb^{207}	8.35	4	3.71	7.91	3.58	1.811	1.189	60.11	1.715
Pb^{208}	11.81	6.92	4.02	12.12	6.7	2.62	2.404	63.93	2.5
Th^{232}	447.8	259.75	40.95	390.67	255.1	93.05	82.51	349.34	102.3
U^{238}	761.75	343.73	85.74	608.7	312.5	158.94	75.66	621.07	167.63
Th/U	0.59	0.76	0.48	0.64	0.82	0.59	1.09	0.56	0.61

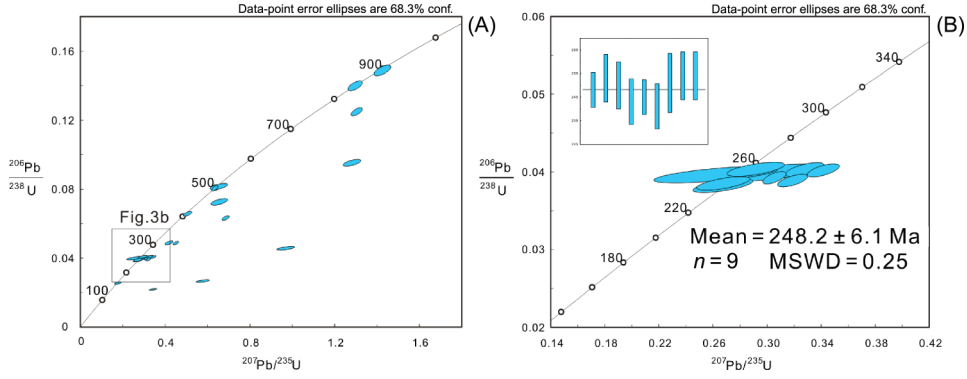

Figure 3. U–Pb concordia plots showing results of LA-ICP-MS dating of zircons from Sample KYB. (A) Part of the zircons; (B) The selected gains.

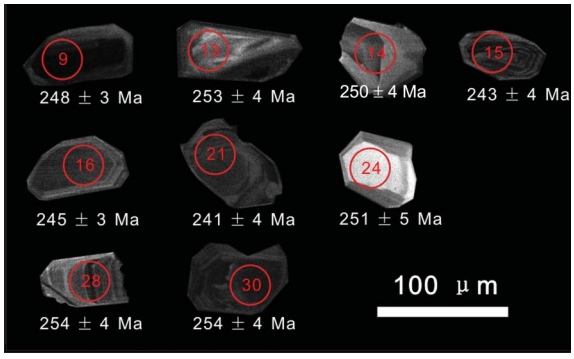

Figure 4. Cathodoluminescence images for the selected zircons from Sample KYB for LA-ICP-MS dating. Red circles indicate the analysed spots.

slightly negative Zr, Hf, and Y anomalies, and variable Pb and Sr anomalies. The Kaiyuan alkaline basalts have constant HFSE ratios: Nb/Th (6.4 to 9.5), Zr/Nb (4.3 to 6.9), Zr/Y (6.1 to 9.7), and Nb/Y (1.0 to 1.7). All of the Kaiyuan alkaline basalts fall into the range of the OIB base in Figure 8. The basalts have uniform chondrite-normalized REE patterns enriched in LREE and without Eu anomaly ($Eu/Eu^* = 0.92–1.19$) (Figure 7B). The basalts have $(La/Yb)_N$ (primitive mantle normalized) values ranging from 10.48 to 24.30 and $(La/Sm)_N$ values from 1.91 to 2.82. The patterns are similar to those of the ocean island basalts (OIB) and the Emeishan high Ti basalts reported by Wang and Zhou (2007) (Figure 7B). However, the Kaiyuan alkaline basalts yield lower HREE and similar MREE (higher MREE/HREE) contents

Table 3. Whole-rock major and trace element compositions of Kaiyuan volcanic rocks.

Layer	Upper							Middle				Lower
Lithology	Basalt						Andesite basalt	Basalt				Alteration basalt
Sample number	11KY-1	11KY-2	11KY-3	11KY-4	11KY-5	11KY-6	11KY-7	11KY-8	11KY-9	11KY-10	11KY-11	11KY-12
Major elements (recalculated to 100 wt.% on a volatile-free basis)												
SiO_2	46.55	44.98	45.09	44.18	45.20	48.36	56.32	45.37	47.42	51.50	45.90	33.51
Al_2O_3	12.13	13.38	13.53	12.80	13.80	14.45	12.33	12.78	14.47	14.33	13.87	10.70
Fe_2O_3	13.96	12.99	16.06	14.03	13.45	14.02	15.02	13.38	14.04	11.20	13.38	9.04
CaO	10.07	10.04	6.87	10.34	9.30	6.65	3.19	10.09	5.06	8.53	9.41	33.42
MgO	7.91	11.52	9.97	11.00	10.40	7.84	6.90	10.30	10.63	6.46	8.83	6.55
Na_2O	2.23	0.83	2.09	1.29	1.90	1.97	1.78	1.52	0.99	2.07	2.30	2.26
K_2O	2.81	2.30	2.05	2.18	1.83	2.64	0.57	2.33	3.03	1.97	2.20	0.56
Cr_2O_3	0.04	0.07	0.04	0.07	0.06	0.03	0.08	0.08	0.08	0.04	0.07	0.03
TiO_2	3.72	3.22	3.65	3.36	3.44	3.49	3.39	3.44	3.54	3.35	3.38	2.55
MnO	0.13	0.16	0.20	0.20	0.16	0.13	0.13	0.17	0.21	0.09	0.22	0.11
P_2O_5	0.34	0.32	0.30	0.41	0.35	0.28	0.26	0.37	0.31	0.35	0.31	0.53
Total	99.89	99.80	99.87	99.85	99.91	99.85	99.98	99.83	99.76	99.89	99.88	99.25
LOI	5.50	6.12	5.78	6.04	6.58	10.75	8.95	6.37	7.86	8.94	6.92	22.60
Trace elements (ppm)												
Sc	24.7	28.6	24.5	23.1	24.6	24.9	22.5	27.9	29.2	27.4	28.1	12.8
V	367	359	337	314	393	352	191	348	366	315	352	167
Cr	228	404	401	417	279	260	533	459	460	305	408	187
Co	45.1	52.7	47.5	52.4	61.4	45.5	44.9	53	55.9	35.8	48.9	26.6
Ni	164.5	231	222	242	241	203	340	239	260	186	223	133.5
Cu	64.8	77.9	51.4	67.8	148.5	131	7.7	84	93.6	86.8	44.6	39
Zn	121	107	104	113	130	93	58	103	114	114	111	68
Ga	16.8	17.65	17.2	18.85	16.3	14.8	18.7	17.9	18.65	16.75	18.15	12.45
Cs	3.28	3.95	1.85	1.42	3.07	1.2	0.33	5.12	7.17	3.29	4.6	6.41
Rb	48.6	37.7	37.4	34.7	34	32.3	9.4	47.2	60.5	34.8	35.3	27
Ba	710	1310	1040	940	490	420	90	770	1840	680	490	3800
Th	3.1	2.7	3.4	3.3	2.4	2.6	3.3	3.7	4	3.3	2.7	3.3
U	0.6	0.6	0.8	0.8	0.5	0.6	0.7	0.7	0.8	0.7	0.6	1.3
Nb	19.9	24.6	28.6	28.8	18.1	21.3	37.7	25.7	27.1	31.3	25.4	30
Ta	1.31	1.67	2.02	2.07	1.2	1.45	2.56	1.79	1.88	2.08	1.71	1.9
Pb	1.2	0.8	3.2	3.1	1.7	8.7	1.7	2.2	1.5	0.7	0.9	1.8
Sr	724	368	544	517	766	698	121	331	308	343	334	1520
Zr	115	131	159.5	170.5	125	134	113	127	135.5	136	135.5	159.5
Hf	3.4	3.9	4.5	4.8	3.8	4.1	3.4	3.9	4.1	4	4	4
Y	19	18.8	17.8	17.5	18.5	18.3	17.5	18.7	19.3	18.2	18.5	15.4

(*Continued*)

Table 3. (Continued).

Layer	Upper							Middle				Lower
Lithology	Basalt						Andesite basalt	Basalt				Alteration basalt
Sample number	11KY-1	11KY-2	11KY-3	11KY-4	11KY-5	11KY-6	11KY-7	11KY-8	11KY-9	11KY-10	11KY-11	11KY-12
REE (ppm)												
La	26.2	27.3	31.1	31.2	23.1	22.5	39.3	28	29.1	28.6	26	35.7
Ce	54.2	57.6	64.4	67.2	51.6	50.6	77.8	58.7	60.8	56	56.1	69.6
Pr	7.14	7.44	8.37	8.66	6.93	6.85	10.8	7.63	7.9	7.11	7.23	8.48
Nd	31.4	32	35.5	37.1	31.2	30.6	45	32.7	33.8	29.6	31.1	34.6
Sm	7.55	7.47	8	8.42	7.75	7.6	10	7.54	7.72	6.54	7.19	7.3
Eu	2.58	2.72	2.52	2.69	2.12	2.38	2.91	2.54	2.81	2.51	2.33	3.19
Gd	6.13	6.22	6.18	6.46	5.92	6.26	7.75	6.07	6.22	5.48	5.95	5.6
Tb	0.99	0.99	0.96	0.99	0.97	1.01	1.16	0.98	1	0.86	0.95	0.84
Dy	4.77	4.77	4.5	4.6	4.77	4.95	5.02	4.71	4.83	4.23	4.59	3.82
Ho	0.85	0.85	0.79	0.79	0.83	0.86	0.79	0.84	0.87	0.76	0.8	0.66
Er	2.11	2.13	1.95	1.95	2.08	2.14	1.83	2.14	2.18	1.96	2	1.63
Tm	0.26	0.25	0.23	0.22	0.25	0.25	0.19	0.26	0.27	0.24	0.23	0.19
Yb	1.54	1.57	1.46	1.42	1.52	1.54	1.16	1.62	1.7	1.47	1.46	1.37
Lu	0.23	0.25	0.23	0.22	0.23	0.22	0.16	0.25	0.28	0.22	0.21	0.24
Ratio												
Mg#	56	66	58	64	63	55	51	63	63	56	59	62
(La/Sm)n	2.24	2.36	2.51	2.39	1.92	1.91	2.54	2.40	2.43	2.82	2.33	3.16
Th/Ce	0.057	0.047	0.053	0.049	0.047	0.051	0.042	0.063	0.066	0.059	0.048	0.047
△Nb	0.26	0.24	0.12	0.06	0.14	0.15	0.52	0.28	0.26	0.30	0.22	0.08

Notes: Mg# = molar MgO/(MgO + FeO) assuming FeO = 0.89* Fe_2O_3; $\Delta Nb = 1.74 + \log(Nb/Y) - 1.92 \log(Zr/Y)$. All the major elements are recalculated to 100% and normalization values follow Sun and McDonough (1989).

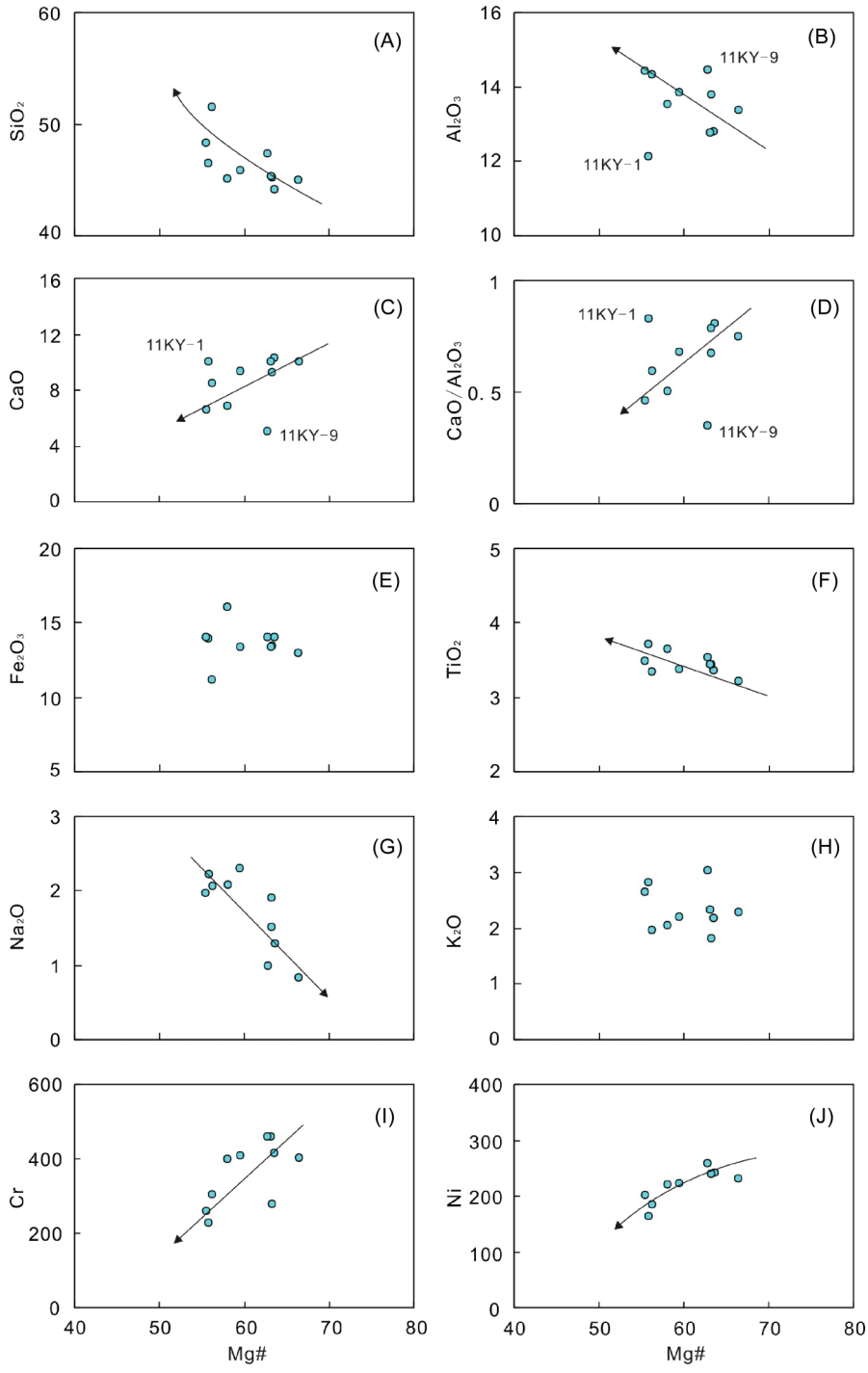

Figure 5. Variation diagrams of major and trace elements in Kaiyuan Anisian basalts.

compared to the Emeishan high Ti basalts, which may imply more garnet in the source of the Kaiyuan alkaline basalts compared to the Emeishan high Ti basalts.

Sr and Nd isotopes

The $^{87}Sr/^{86}Sr$ and $^{143}Nd/^{144}Nd$ ratios of the selected samples are listed in Table 5. The initial isotopic ratios are corrected to a nominal age of 248 Ma based on the LA-ICP-MS zircon U-Pb result of the KYB sample.

Most of the selected basalt samples have negative $\varepsilon Nd(t)$ values (except 11KY-11) ranging from −2.2 to −0.1 and $(^{87}Sr/^{86}Sr)_i$ values ranging from 0.70524 to 0.70637. There is no correlation between $(^{87}Sr/^{86}Sr)_i$ and LOI (not shown), which suggests that the high $(^{87}Sr/^{86}Sr)_i$ values are not attributable to weathering or alteration.

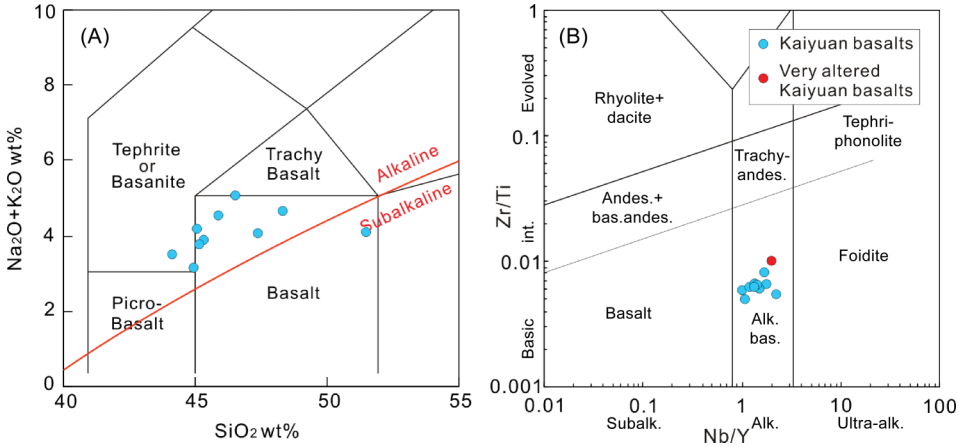

Figure 6. (A) Total alkali–silica (TAS) diagram for the Kaiyuan volcanics samples. The dotted line distinguishes alkaline basalts from subalkaline basalts, base on (Le Bas *et al.* 1986); (B) Zr/Ti *versus* Nb/Y classification diagram of Winchester and Floyd (1977) modified by Pearce (1996).

Table 4. The CIPW norm mineral calculation (volume %) of Kaiyuan basalts.

Sample number	11KY-1	11KY-2	11KY-3	11KY-4	11KY-5	11KY-6	11KY-8	11KY-9	11KY-10	11KY-11
Quartz	0	0	0	0	0	0	0	0	4.2	0
Plagioclase	45.0	37.9	37.1	35.5	45.5	30.7	40.4	36.1	46.6	44.7
Orthoclase	18.8	16.6	16.9	15.8	14.9	20.2	15.8	21.9	13.8	13.1
Nepheline	0	0	1.2	2	0	4.7	3.4	0	0	0.7
Corundum	0	0	0	0	0	0	0	0.9	0	0
Diopside	6.4	16.6	20.3	19.9	8.2	25.1	17.9	0	12	15.3
Hypersthene	16.9	4.9	0	0	3.6	0	0	29.6	17.6	0
Olivine	6.9	18	18.3	20.4	21.2	12.7	16.4	5.2	0	20
Ilmenite	4.3	4.0	4.3	4.2	4.6	4.6	4.2	4.4	4.1	4.3
Magnetite	1.2	1.1	1.2	1.2	1.4	1.2	1.2	1.2	0.9	1.2
Apatite	0.6	0.7	0.8	0.9	0.7	0.8	0.7	0.7	0.8	0.8
Total	100	100	100	100	100	100	100	100	100	100

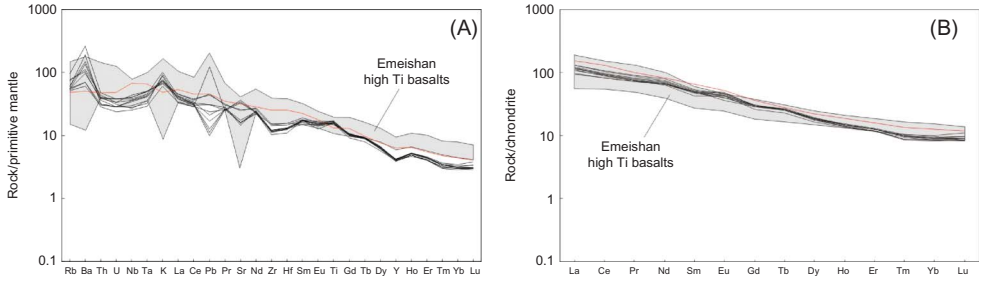

Figure 7. Primitive mantle-normalized trace element patterns (A) and chondrite-normalized REE patterns (B) of basalt samples from the Kaiyuan area. Normalization and OIB (red line) values follow Sun and McDonough (1989).

From Figure 9, the Sr-Nd isotopic compositions of the Kaiyuan alkaline basalts define a negative correlation in the Sr-Nd isotopic plot and lie in the range of the mantle array and overlap with the Emeishan flood basalts.

Discussion

Onset of basalt eruption

The KYB sample contains a large number of inherited zircons with older ages. Three samples (KYB-03, KYB-10, and KYB-22) show anomalously young $^{206}Pb/^{238}U$ ages and are discordant with the other ages. Those zircons commonly have several cracks. Therefore, the anomalous ages of those three zircons are most likely caused by the radioactive origin of Pb loss.

Nine zircons yield an age of 248 ± 6 Ma. These zircons not only have magmatic morphological characteristics, oscillatory zoning (Figure 4), magmatic Th/U ratios, and their linear correlation but also demonstrate similar

trends of REE and conglomerate age. The above facts indicate that these zircons were formed in a single magmatic event. We consider this centralized age to be the best estimate of the crystallization age of the zircons, which also represents the eruption age of the basalts (Song and Qiao 2008).

The Ti-in-zircon thermometer has been widely used for calculating the crystal temperature of zircon (Watson and Harrison 2005; Watson *et al.* 2006; Baldwin *et al.* 2007; Anderson *et al.* 2008; Fu *et al.* 2008). We have calculated the crystal temperature of the KYB zircons and compared it with the massive data reported by Fu *et al.* (2008). The average temperature of the KYB zircons is 832°C (Figure 10). This high temperature is close to the calculated temperature of the zircon in mafic rocks (758°C) and further exceeds the temperature of the zircon in intermediate and felsic igneous rocks (653°C). This finding suggests that those zircons were formed in mafic melts.

Trace element abundances in igneous zircons are sensitive to the source rock type and the crystallization environment. According to the zircon trace-element CART tree for source rock estimation (Belousova *et al.* 2002), the results establish that the source rock for these zircons is basalt.

Based on the above evidence, we believe that the selected zircons from the KYB sample are those that formed in the basaltic melt and the $^{206}Pb/^{238}U$ weighted mean age of the zircons, i.e. 248 ± 6 Ma (MSWD = 0.25, n = 9), is regarded as the eruption age of the Kaiyuan alkaline basalts.

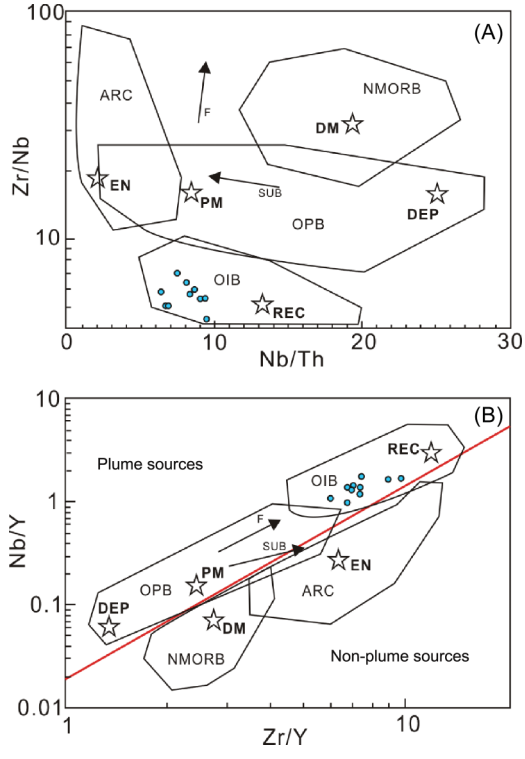

Figure 8. Diagram showing mantle compositional components and fields for basalts from various tectonic settings (Weaver 1991; Fitton *et al.* 1997; Condie 2003). (A) Nb/Th–Zr/Nb; (B) Zr/Y–Nb/Y.

Petrogenesis and magma evolution

Alteration

The high LOI (>5%) of the Kaiyuan basalt samples display relatively strong alteration. The serpentinization and chloritization of the mafic minerals are observed both in hand specimens and under the microscope. However, the physical and chemical alterations commonly removed the mobile elements, such as Rb, Ba, and K. The HFSE and REE remained immobile during the process of metamorphism or hydrothermal alteration, and therefore, the ratios between these elements remained constant. The consistent linear correlations between the La and the other REE and HFSE (not shown) indicate that these elements are relatively immobile during the alteration process. Therefore, the concentrations of HFSE and REE reported here are assumed to represent suitable proxies to evaluate the petrogenesis of the Kaiyuan alkaline basalts (Staudigel and Hart 1983; Wang and Zhou 2007).

Fractional crystallization and crustal contamination

The Kaiyuan alkaline basalts with MgO contents ranging from 6.46 to 11.52 wt.% and Mg# ranging from 55 to 66, which are lower than the Mg# (68–72) of primitive basaltic magma (Green 1976), suggest that they had experienced magma evolution prior to the lava eruption. The fractionation processes can be identified from the SiO_2 versus Nb/La plots (Figure 11A). The AFC process may increase SiO_2 and decrease HSFE, including Nb, causing lower Nb/La ratios. In contrast, the FC processes do not change the Nb/La ratios (Ernst *et al.* 1988; Xiao *et al.* 2008). As evident from Figure 11A, a constant Nb/La ratio for all the samples suggests FC had occurred. It can be inferred from Figures 6A, 6B, and 6J that olivine was fractionated (except the 11KY-1 and 11KY-9) and Figures 6D and 6I indicate that clinopyroxene was fractionated as well.

The Nb/La value of the Kaiyuan alkaline basalts (Figure 11A) fall in the range between the OIB (1.3) and the upper crust (0.39), and the occurrence of inherited zircons indicate that crustal contamination has taken place. The crustal contaminated basalts typically have Th/Ce ratios >0.05 (Kerrich *et al.* 1999a, 1999b; Condie 2003). The mean Th/Ce ratio of the Kaiyuan alkaline basalts presented in this study is 0.051 (Table 3). Moreover, we can draw a conclusion from Figure 9 that 5–10% of the middle crust of the Yangzte block was added into the magma of the Kaiyuan alkaline basalts during its ascent.

Table 5. Sr–Nd isotopic compositions of Kaiyuan basalts.

Sample	Rb	Sr	$^{87}Sr/^{86}Sr$	2σ	$(^{87}Sr/^{86}Sr)_i$	Sm	Nd	$^{143}Nd/^{144}Nd$	2σ	$(^{143}Nd/^{144}Nd)_i$	εNd(t)
11KY-2	37.7	368	0.70738	6	0.70637	7.47	32	0.512543	1	0.512204	−2.2
11KY-3	37.4	544	0.705943	7	0.70583	8	35.5	0.512520	3	0.512265	−1
11KY-4	34.7	517	0.705961	4	0.70633	8.42	37.1	0.512525	2	0.512314	−0.1
11KY-5	32.3	698	0.706619	7	0.70524	7.6	30.6	0.512495	5	0.512299	−0.4
11KY-6	34	766	0.706522	5	0.70528	7.75	31.2	0.512534	2	0.512302	−0.3
11KY-8	47.2	331	0.707826	6	0.70607	7.54	32.7	0.512431	2	0.512290	−0.6
11KY-10	34.8	343	0.706864	6	0.70615	6.54	29.6	0.512482	2	0.512251	−1.3
11KY-11	35.3	334	0.706392	3	0.70531	7.19	31.1	0.512575	2	0.512347	0.6

Note: $(^{87}Sr/^{86}Sr)_i$, $(^{143}Nd/^{144}Nd)_i$, and εNd(t) were calculated for 248 Ma.

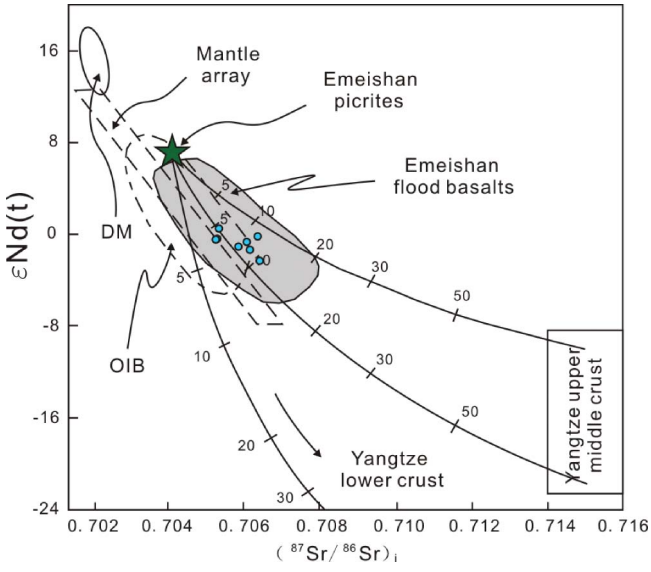

Figure 9. εNd (t) (t = 248 Ma) values *versus* initial $(^{87}Sr/^{86}Sr)_i$ diagram for Kaiyuan alkaline basalts after Wang and Zhou (2007). DM (depleted mantle), mantle array and EMI and EMII trends are after Zindler and Hart (1986). Bulk Earth data from Depaolo (1988). OIB data are from Wilson (1989). The Yangtze upper/middle crust and lower crust data are from Gao *et al.* (1999), Ma *et al.* (2000) and Chen and Jahn (1998). The numbers indicate the percentages of participation of the crustal materials. The calculated parameters of Nd (ppm), εNd (t), Sr (ppm), and $(^{87}Sr/^{86}Sr)_i$ are 4.4, +7, 102, and 0.704 from picrites in northern Vietnam as parental magmas; 20, −22, 220, 0.715, and 20, −10, 220, 0.715 as two components of the Yangtze middle/upper crust.

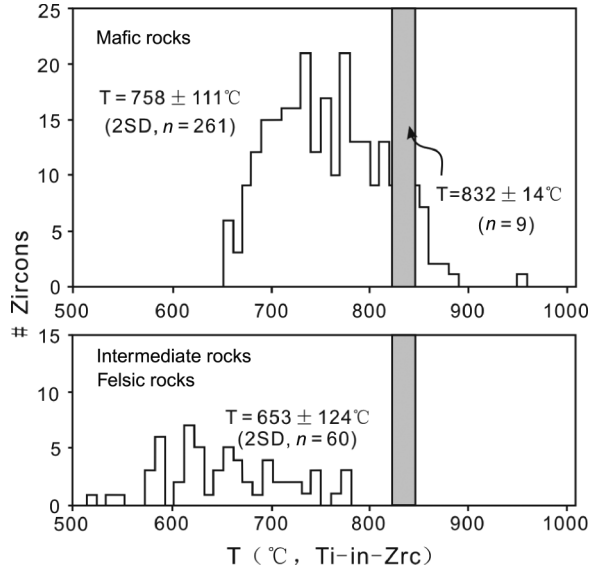

Figure 10. Histograms of Ti–in–zircon temperatures for KYB zircons (gray pillar), mafic rocks, and intermediate and felsic igneous rocks. Abbreviations in parentheses: SD = standard deviation, n = number of zircon grains analysed. Modified from Fu *et al.* (2008).

Mantle source, partial melting, and plume indications

$\Delta Nb = 1.74 + \log(Nb/Y) - 1.92 \log(Zr/Y)$ is a fundamental source characteristic and is insensitive to the effects of variable degrees of mantle melting, source depletion through melt extraction, crustal contamination of the magmas, or subsequent alteration, according to Fitton *et al.* (1997). All Icelandic basalts have $\Delta Nb > 0$, whereas all N-MORB have $\Delta Nb < 0$. The Kaiyuan alkaline basalts have ΔNb values of 0.06 to 0.30 (Table 3), which indicates source enrichment.

Previous studies have suggested that using immobile incompatible element ratios is feasible to trace the mantle source of basalts (Weaver 1991; Fitton *et al.* 1997; Baksi 2001; Condie 2003; Fitton *et al.* 2003; Condie 2005; Willbold and Stracke 2006; Pearce 2008). The Kaiyuan alkaline basalts show LREE-enriched patterns (Figure 7B) and OIB-like immobile incompatible element ratios (Figures 8A and 8B), which implies that the Kaiyuan alkaline basalts originate from the enriched mantle source (similar source of OIB).

The hypotheses for OIB and OIB-like basalt formation fall into three categories: (1) mantle plumes (Hofmann and White 1982); (2) dispersed blobs or streaks of incompatible-element-enriched material in the depleted upper mantle (Niu 2008; Pilet *et al.* 2008); and (3) a layer of shallow mantle (the perisphere; Anderson 1995) that is enriched in incompatible elements compared to the deeper parts of the upper mantle.

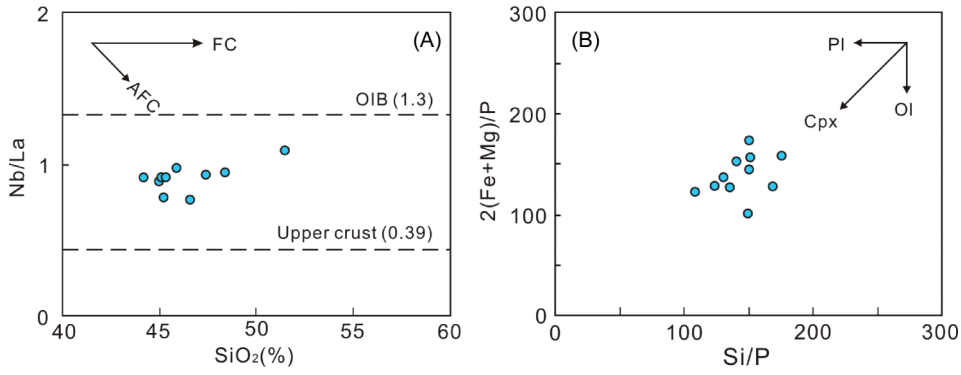

Figure 11. Nb/La *versus* SiO_2 plots (A) and 2(Fe + Mg)/P *versus* Si/P plots (B). References: Ernst *et al.* (1988); Xiao *et al.* (2008). Average values for OIB are after Sun and McDonough (1989). Average value for upper crust is after Rudnick and Gao (2003).

The spatial location and the geochemistry, similar to the Emeishan high Ti basalts, indicate that the Kaiyuan alkaline basalts are related to the Emeishan plume event. Moreover, all of the plots of the Kaiyuan alkaline basalts fall in the range of the Emeishan flood basalts, as is evident from Figure 9. This similarity suggests that the Kaiyuan alkaline basalts were also derived from the same plume-type source as the Emeishan flood basalts.

Garnet has a high partition coefficient for Y ($D_{garnet/melt}$ = 3.1) relative to Ti ($D_{garnet/melt}$ = 0.29), and Lu ($D_{garnet/melt}$ = 7.1) compared to La ($D_{garnet/melt}$ = 0.0016) (Johnson 1998). Therefore, the high Ti/Y ratios (average of 1123) and the REE pattern (enriched in LREE and depleted in HREE) of the Kaiyuan alkaline basalts indicate a mantle source at a garnet-stable field.

The degree of partial melting of the mantle source could be assessed by the diagram of Sm *versus* Sm/Yb (Qi and Zhou 2008) using the non-modal batch melting equations of Shaw (1970). The samples with high MgO (>8 wt.%) were selected to estimate the degree of partial melting because those may bear the information about the partial melting and source history. From Figure 12, we conclude that the Kaiyuan alkaline basalts originated from 4% to 6% partial melting of garnet peridotite.

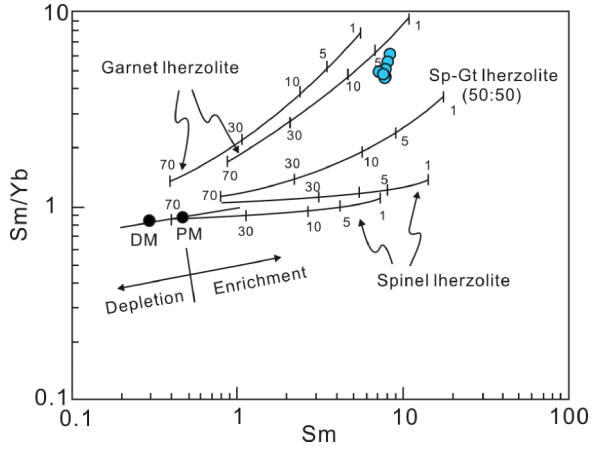

Figure 12. Plots of Sm/Yb *versus* Sm showing melt curves for Kaiyuan alkaline basalts, after Qi and Zhou (2008).

Tectonic setting

The Anisian basaltic lavas erupted through the Pingtang–Kaiyuan fault and were hosted in the Gejiu formation in the Kaiyuan, Gejiu, and Funing areas (YBGMR 1982). Based on the characteristics of petro-chemistry and rock occurrence, Zheng and Liu (1993), Xue (2002) suggested that these Anisian basaltic lavas were formed in the extensional tectonic setting (rift) within the continent during the Triassic period.

From the study of the lithofacies palaeogeography, Luo *et al.* (2008) considered the Kaiyuan–Gejiu district to be a semi-restricted gulf during the Triassic period. The gulf had a barrier rim in the southwest and ancient land towards the northwest and south. The water depths increased dramatically in the gulf and deposited approximately 5000 m of deepwater limestone in the area during the Triassic period. According to the calculation from the fluid inclusions of Gejiu Anisian basalt-related ore, the ore-forming depth was from 6050 to 7050 m, indicating a deep-sea rift environment (Lu 2008). Based on the evidence above, we consider that the Kaiyuan alkaline basalts were related to a rift event during the Triassic period.

Many diagrams can be used for the tectonic discrimination of basic lavas erupted in most tectonic environments (Pearce and Cann 1973; Wood 1980; Meschede 1986). The Nb-Zr-Y diagram (Figure 13A), Ti-Zr-Y diagram (Figure 13B), and Hf-Th-Ta diagram (Figure 13C) imply that the Kaiyuan alkaline basalts are within-plate basalts (OIB and CFB). Therefore, we propose that the Kaiyuan alkaline basalts, which have continental basalt characteristic, were erupted within the Yangzte craton at 248 Ma.

Based on the above discussion, the Kaiyuan alkaline basalts were related to a rift event and erupted within the Yangzte craton at 248 Ma. The trace element ratios and isotope ratios of the Kaiyuan alkaline basalts are similar to

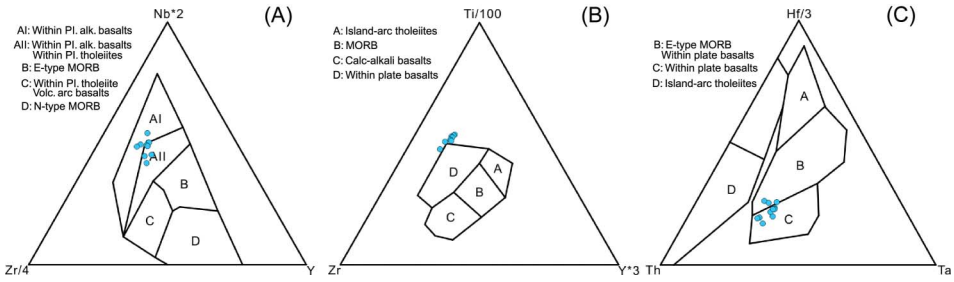

Figure 13. Tectonic setting discrimination diagrams for the Qilinshan basalts. (A) Nb-Zr-Y diagram (Meschede 1986); (B) Ti-Zr-Y diagram (Pearce and Cann 1973), (C) Hf-Th-Ta diagram (Wood 1980).

those of the Emeishan high Ti basalts, which implies that the Kaiyuan alkaline basalts were derived from the same plume-type source as the Emeishan flood basalts. However, the young eruption age (248 ± 6 Ma) excludes the possibility that the Kaiyuan alkaline basalts formed during the main event of ECFB (260–257 Ma by Shellnutt *et al.* 2012). More likely, it could have been the result of post-ELIP relaxation and remelting of the Emeishan fossil plume head at 248 Ma.

Tectonic setting comparison between the Red Sea and Kaiyuan

The coincidence between the hotspots, continental flood basalts, and rifts has long been recognized (Morgan 1971; Courtillot *et al.* 1999). A promising area for studying continental rift processes and the transition between continental rift and sea-floor spreading is the Afar volcanic province, because it is currently undergoing continental break-up. We have the opportunity to assess a rift history that includes both a well-defined plume that was subsequently split by extensional structures, and segments of the same rifts that are far removed from significant coeval volcanism. The timing of the various phases of this plume-rift system is now relatively well known, particularly in comparison to other ancient rift systems.

History of the tectonic and magmatic events in the Red Sea area

Plume-related basaltic trap volcanism initiated at Afar, Derudeb in NE Sudan, and SW Yemen at 31 Ma and continued up to 25 Ma. This early magmatism occurred without significant regional extension. However, this pre-rift magmatism may have provided stress concentration or local weakening of the continental lithosphere (e.g. Malkin and Shemenda 1991; Bellahsen *et al.* 2004) that triggered a rift event that was already in the making.

The second phase of the magmatism accompanied strong extension and deposition that occurred at 24 Ma (slightly older in southernmost Yemen). It is well documented that the transverse tectonic structures of the Afar Depression are characterized by alkaline basaltic volcanism (Teklay *et al.* 2010 and references therein). These syn-rift alkaline volcanisms, commonly hundreds of metres thick, represent outpourings through the continental crust that were precursors to the rift of plate divergence (Waltham 2005).

Throughout the Red Sea, the principal phase of the rift shoulder uplift and rapid syn-rift subsidence followed shortly thereafter at 20 Ma. Water depths increased dramatically and sedimentation changed to predominantly Globigerina-rich marl and deepwater limestone (Bosworth *et al.* 2005).

History of tectonic and magmatic events in the Kaiyuan area

As evident from the Red Sea–Gulf of Aden rift system, we can reconstruct the ancient tectonic and magmatic events for the western margin of the Yangzte craton.

The new data from the ELIP indicate that plume-related magmatism was likely to have been short-lived (of the order of 2 million years) and must have ended by ~257 Ma (Shellnutt *et al.* 2012). The magmatism may have provided stress concentration or local weakening of the continental lithosphere on the southwestern margin of the Yangtze crust.

At 248 Ma, the second phase of alkaline magmatism accompanied strong post-ELIP relaxation of the Yangtze crust that had occurred as Shellnutt and Zhou (2007) and Shellnutt *et al.* (2008) had proposed. This process was likely responsible for the melting of the underplated Emeishan plume head mafic rocks emplaced at ~260 Ma and yielded the Kaiyuan alkaline basalts at 248 ± 6 Ma.

Despite the volumetrically negligible amounts, when compared to the volume of the flood basalts, the Kaiyuan alkaline basalts were a probe for a Red Sea-like rift system. Water depths increased dramatically in the Kaiyuan-Gejiu gulf (Xue 2002) and deposited approximately 5000 m of deepwater limestone in the area during the Triassic period.

In all cases, an active component (a plume and resulting flood basalt) is a prerequisite for the breakup of a major oceanic basin. Additionally, rift formation needs to be accommodated by plate–boundary forces, and it is influenced by pre-existing heterogeneities in the lithospheric structure (Courtillot *et al.* 1999). The Kaiyuan

rift system only survived for a short period because the rift formation was against the ambient plate–boundary forces. The Ailaoshan–Nan–Uttaradit back-arc basin was closed when the Simao terrane collided back with the South China/Indochina block in the Middle to early Late Triassic base on the palaeogeographic reconstructions from Metcalfe (2006) (Figure 14). Therefore, the Kaiyuan rift disappeared in the Late Triassic period.

Appropriate scenario of the Kaiyuan petrological process

In summary, we put forward an appropriate scenario for the Kaiyuan petrological process and the tectonic setting during that period (Figure 15).

The ELIP was approximately emplaced at 260 Ma and ended at 257 Ma. It had provided the stress concentration or local weakening of the Yangtze continental lithosphere that had triggered a rift event at 248 Ma, characterized by the eruption of the Kaiyuan alkaline basalts. Those basalts were formed by the melting of the fossil plume-head (Xu *et al.* 2004; Shellnutt *et al.* 2008), and therefore, possess a geochemical signature similar to the Emeishan flood basalts. Because the Simao terrane collided back with the South China/Indochina block in the Middle to early Late Triassic period, the rift system came against plate–boundary forces and disappeared quickly in the Late Triassic.

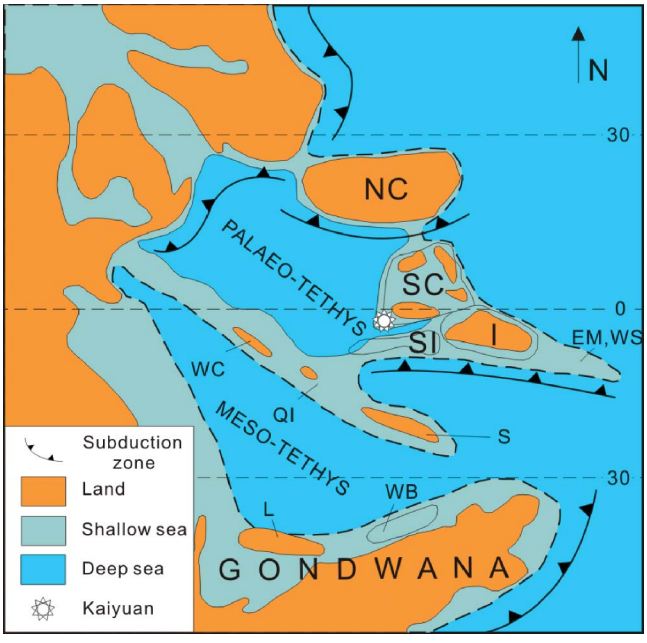

Figure 14. Palaeogeographic reconstructions of the Tethyan region for 255 Ma, and relative positions of the East and Southeast Asian terranes, and distribution of land and sea (Metcalfe 2006). SC = South China; I = Indochina; NC = North China; SI = Simao; S = Sibumasu; WB = West Burma; QI = Qiangtang; *L* = Lhasa; WC = Western Cimmerian Continent.

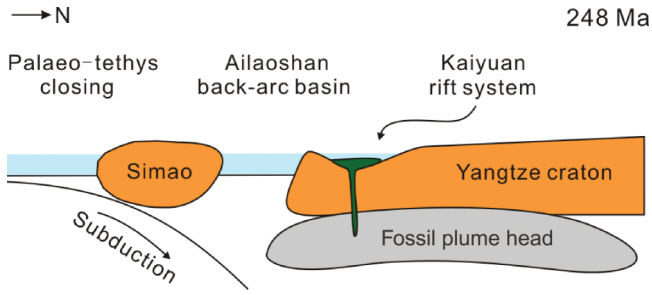

Figure 15. Schematic diagram illustrating the tectonic setting (248 Ma) and genesis of the Kaiyuan alkaline basalts.

Conclusions

Combined with previous geological, petrological, and geochemical studies of the alkaline basalts of the Kaiyuan area, our conclusions are summarized below.

LA-ICP-MS zircon U-Pb dating reveals a crystallization age of these alkaline basalts at 248 ± 6 Ma (MSWD = 0.25, $n = 9$).

The Kaiyuan alkaline basalts display enriched REE patterns and trace and isotope element geochemical characteristics, similar to those of the ocean island basalts and Emeishan high Ti basalts. The geochemistry could have been a result of 4–6% partial melting of a garnet peridotite protolith, involving significant early crystallization of clinopyroxene, and more than 5% crustal contamination.

The Kaiyuan alkaline basalts were the result of post-ELIP relaxation and remelting of the ELIP fossil plume head which had been emplaced at ~260 Ma.

A Red Sea-like rift system was generated along the southwestern margin of the Yangzte craton at 248 Ma. The Simao terrane collided with the South China/Indochina block in Middle to early Late Triassic time, causing the disappearance of the rift system, leaving behind the Kaiyuan alkaline basalts.

Acknowledgements

This study is financially supported by the Crisis Mines Continued Resources Exploration Project of the China Geological Survey (No. 2008186); The 12th Five-Year Plan project of the State Key Laboratory of Ore-deposit Geochemistry, the Chinese Academy of Sciences (SKLODG-ZY125-02) and the National Natural Science Foundation of China (No. 41073032). We appreciate the assistance of Jing Hu, Guangping BAO, and Yan Huang for trace element analyses and to Xiaobiao Li for the Rb-Sr isotope ratio analyses. We are grateful to Wenbo Li and Cheng Xu for advice on the manuscript.

References

Ali, J.R., Fitton, J.G., and Herzeberg, C., 2010, Emeishan large igneous province (SW China) and the mantle–plume up–doming hypothesis: Journal of the Geological Society, v. 167, p. 953–959.

Ali, J.R., Thompson, G.M., Zhou, M.F., and Song, X.Y., 2005, Emeishan large igneous province, SW China: Lithos, v. 79, p. 475–489.

Andersen, T., 2002, Correction of common lead in U–Pb analysis that do not report ^{204}Pb: Chemical Geology, v. 192, p. 59–79.

Anderson, D.L., 1995, Lithosphere, asthenosphere, and perisphere: Reviews of Geophysics, v. 33, p. 125–149.

Anderson, J.L., Barth, A.P., Wooden, J.L., and Mazdab, F., 2008, Thermometers and thermobarometers in granitic systems: Reviews in Mineralogy and Geochemistry, v. 69, p. 121–142.

Baksi, A.K., 2001, Search for a deep–mantle component in mafic lavas using a Nb–Y–Zr plot: Canadian Journal of Earth Sciences, v. 38, p. 813–824.

Baldwin, J.A., Brown, M., and Schmitz, M.D., 2007, First application of titanium–in–zircon thermometry to ultrahigh–temperature metamorphism: Geology, v. 35, p. 295.

Bellahsen, N., Faccenna, C., Funiciello, F., Daniel, J.M., and Jolivet, L., 2004, Why did Arabia separate from Africa? Insights from 3–D laboratory experiments: Earth and Planetary Science Letters, v. 216, p. 365–381.

Belousova, E.A., Griffin, W.F., O'Reilly, S.Y., and Fisher, N.I., 2002, Igneous zircon: Trace element composition as an indicator of source rock type: Contributions to Mineralogy and Petrology, v. 143, p. 602–622.

Bosworth, W., Huchon, P., and McClay, K., 2005, The Red sea and gulf of Aden basins: Journal of African Earth Sciences, v. 43, p. 334–378.

Chen, J.F., and Jahn, B.M., 1998, Crustal evolution of southeastern China, Nd and Sr isotopic evidence: Tectonophysics, v. 284, p. 101–133.

Condie, K.C., 2003, Incompatible element ratios in oceanic basalts and komatiites, tracking deep mantle sources and continental growth rates with time: Geochemistry Geophysics Geosystems, v. 4, no. 1, p. 1005, doi: 10.1029/2002GC000333.

Condie, K.C., 2005, High field strength element ratios in Archean basalts, a window to evolving sources of mantle plumes?: Lithos, v. 79, p. 491–504.

Courtillot, V., Jaupart, C., Manighetti, I., Tapponnier, P., and Besse, J., 1999, On causal links between flood basalts and continental breakup: Earth and Planetary Science Letters, v. 166, p. 177–195.

Depaolo, D.J., 1988, Neodymium isotope geochemistry, an introduction: New York, Springer Verlag, 187 p.

Ernst, R.E., Fowler, A.D., and Pearce, T.H., 1988, Modeling of igneous fraction and other processes using Pearce diagrams: Contributions to Mineralogy and Petrology, v. 100, p. 12–18.

Fitton, J.G., Saunders, A.D., Kempton, P.D., and Hardarson, B.S., 2003, Does depleted mantle form an intrinsic part of the Iceland plume?: Geochemistry Geophysics Geosystems, v. 4, no. 3, p. 1032, doi: 10.1029/2002GC000424, 3.

Fitton, J.G., Saunders, A.D., Norry, M.J., Hardarson, B.S., and Taylor, R.N., 1997, Thermal and chemical structure of the Iceland plume: Earth and Planetary Science Letters, v. 153, p. 197–208.

Fu, B., Page, F.Z., Cavosie, A.J., Fournelle, J., Kita, N.T., Lackey, J.S., Wilde, S.A., and Valley, J.W., 2008, Ti–in–zircon thermometry: Applications and limitations: Contributions to Mineralogy and Petrology, v. 156, p. 197–215.

Gao, S., Lin, W.L., and Qiu, Y.M., 1999, Contrasting geochemical and Sm–Nd isotopic compositions of Archaean metasediments from the Kongling high–grade terrain of the Yangtze craton, evidence for cratonic evolution and redistribution of REE during crustal anatexis: Geochimica et Cosmochimica Acta, v. 63, p. 2071–2088.

Green, D.H., 1976, Experimental testing of "equilibrium" partial melting of peridotite under water–saturated, high–pressure conditions: The Canadian Mineralogist, v. 14, p. 255–268.

Hanski, E., Kamenetsky, V.S., Luo, Z.Y., Xu, Y.G., and Kuzmin, D.V., 2010, Primitive magmas in the Emeishan large igneous province, southwestern China and northern Vietnam: Lithos, v. 119, p. 75–90.

Hofmann, A.W., and White, W.M., 1982, Mantle plumes from ancient oceanic crust: Earth and Planetary Science Letters, v. 57, p. 421–436.

Johnson, K.T.M., 1998, Experimental determination of partition coefficients for rare earth and high–field–strength elements between clinopyroxene, garnet, and basaltic melt at high pressures: Contributions to Mineralogy and Petrology, v. 133, p. 60–68.

Kerrich, R., Polat, A., Wyman, D., and Hollings, P., 1999a, Trace element systematics of Mg–, to Fe–tholeiitic basalt suites of the Superior Province, implications for Archean mantle reservoirs and greenstone belt genesis: Lithos, v. 46, p. 163–187.

Kerrich, R., Wyman, D., Hollings, P., and Polat, A., 1999b, Variability of Nb/U and Th/La in 3.0 to 2.7 Ga Superior Province ocean plateau basalts, implications for the timing of continental growth and lithosphere recycling: Earth and Planetary Science Letters, v. 168, p. 101–115.

Le Bas, M.J., Le Maitre, R.W., Streckeisen, A., and Zanettin, B., 1986, A chemical classification of volcanic rocks based on the total alkali–silica diagram: Jourary of Petrology, v. 27, p. 745–750.

Liu, Y.S., Gao, S., Hu, Z.C., Gao, C.G., Zong, K.Q., and Wang, D., 2010, Continental and oceanic crust recycling-induced melt-peridotite interactions in the Trans-North China Orogen, U–Pb dating, Hf isotopes and trace elements in zircons of mantle xenoliths: Journal of Petrology, v. 51, p. 537–571.

Lu, H.J., 2008, An approach to geologic features and genesis of basic volcanic rock–type copper deposit in Eastern Gejiu zone: Nonferrous Metals, v. 60, p. 22–33 (in Chinese with English abstract).

Ludwig, K.R., 2003, ISOPLOT 3.0, a geochronological toolkit for microsoft excel: Berkeley Geochronology Center Special publication, no. 4, Berkeley, CA, 71 p.

Luo, R.S., Yang, X.S., Zhang, S.Y., and Wang, W.X., 2008, Lithofacies and paleogeographic conditions for Gejiu cassiterite bearing sulfides deposit, Yunnan: Geology and Prospecting, v. 44, p. 36–41 (in Chinese with English abstract).

Ma, C.Q., Ehlers, C., and Xu, C.H., 2000, The roots of the Dabieshan ultrahigh–pressure metamorphic terrain, constraints from geochemistry and Nd–Sr isotope systematics: Precambrian Research, v. 102, p. 279–301.

Malkin, B.V., and Shemenda, A.I., 1991, Mechanism of rifting, considerations based on results of physical modeling and on geological and geophysical data: Tectonophysics, v. 199, p. 191–210.

Meschede, M., 1986, A method of discrimination between different types of mid–ocean ridge basalts and continental tholeiites with the Nb–Zr–Y diagram: Chemical Geology, v. 56, p. 207–218.

Metcalfe, I., 2006, Palaeozoic and Mesozoic tectonic evolution and palaeogeography of East Asian crustal fragments: The Korean Peninsula in context: Gondwana Research, v. 9, p. 24–46.

Morgan, W.J., 1971, Convection plumes in the lower mantle: Nature, v. 230, p. 42–43.

Niu, Y.L., 2008, The origin of alkaline lavas: Science, v. 320, p. 883–884.
Pearce, J.A., 1996, A user's guide to basalt discrimination diagrams, *in* Wyman, D.A., ed., Trace element geochemistry of volcanic rocks, applications for massive sulphide exploration: Geological Association of Canada, Short Course Notes, 12, p. 79–113.
Pearce, J.A., 2008, Geochemical fingerprinting of oceanic basalts with applications to ophiolite classification and the search for Archean oceanic crust: Lithos, v. 100, p. 14–48.
Pearce, J.A., and Cann, J.R., 1973, Tectonic setting of basic volcanic rocks determined using trace element analyses: Earth and Planetary Science Letters, v. 19, p. 290–300.
Pilet, S., Baker, M.B., and Stolper, E.M., 2008, Metasomatized lithosphere and the origin of alkaline lavas: Science, v. 320, p. 916–919.
Qi, L., and Zhou, M.-F., 2008, Platinum-group elemental and Sr–Nd–Os isotopic geochemistry of Permian Emeishan flood basalts in Guizhou Province, SW China: Chemical Geology, v. 248, p. 83–103.
Rudnick, R.L., and Gao, S., 2003, Composition of the continental crust, *in* Rudnick, R.L., ed., The crust, Treatise in geochemistry, Volume 3: Oxford, Elsevier-Pergamon, p. 1–64.
Shaw, D.M., 1970, Trace element fractionation during anatexis: Geochimica et Cosmochimica Acta, v. 34, p. 237–243.
Shellnutt, J.G., Denyszyn, S.W., and Mundil, R., 2012, Precise age determination of mafic and felsic intrusive rocks from the Permian Emeishan large igneous province (SW China): Gondwana Research, v. 22, p. 118–126.
Shellnutt, J.G., and Jahn, B.M., 2010, Formation of the Late Permian Panzhihua plutonic–hypabyssal–volcanic igneous complex, Implications for the genesis of Fe–Ti oxide deposits and A–type granites of SW China: Earth and Planetary Science Letters, v. 289, p. 509–519.
Shellnutt, J.G., and Jahn, B.M., 2011, Origin of Late Permian Emeishan basaltic rocks from the Panxi region (SW China), implications for the Ti–classification and spatial–compositional distribution of the Emeishan flood basalts: Journal of Volcanology and Geothermal Research, v. 199, p. 85–95.
Shellnutt, J.G., and Zhou, M.-F., 2007, Permian peralkaline, peraluminous and metaluminous A–type granites in the Panxi district, SW China, their relationship to the Emeishan mantle plume: Chemical Geology, v. 243, p. 286–316.
Shellnutt, J.G., Zhou, M.-F., Yan, D.P., and Wang, Y.B., 2008, Longevity of the Permian Emeishan mantle plume (SW China): 1 Ma, 8 Ma or 18 Ma?: Geological Magazine, v. 145, no. 3 p. 373–388.
Song, B., and Qiao, X., 2008, Ages of zircons from basalt of Erdaogou formation and diabase dyke swarms in Northern Liaoning: Earth Science Frontiers, v. 15, p. 250–262.
Song, X.-Y., Qi, H.-W., Robinson, P.T., Zhou, M.-F., Cao, Z.-M., and Cheng, L.-M., 2008, Melting of the subcontinental lithospheric mantle by the Emeishan mantle plume; evidence from the basal alkaline basalts in Dongchuan, Yunnan, Southwestern China: Lithos, v. 100, p. 93–111.
Staudigel, H., and Hart, S.R., 1983, Alteration of basaltic glass: Mechanisms and significance for the oceanic crust–seawater budget: Geochimica et Cosmochimica Acta, v. 47, p. 337–350.
Sun, S.S., and McDonough, W.F., 1989, Chemical and isotopic systematics of oceanic basalts, implications for mantle composition and processes: Geological Society, London: Special Publications, 42, p. 313–345.
Teklay, M., Scherer, E.E., Mezger, K., and Danyushevsky, L., 2010, Geochemical characteristics and Sr–Nd–Hf isotope compositions of mantle xenoliths and host basalts from Assab, Eritrea, implications for the composition and thermal structure of the lithosphere beneath the Afar depression: Contributions to Mineralogy and Petrology, v. 159, p. 731–751.
Waltham, T., 2005, Extension tectonics in the Afar Triangle: Geology Today, v. 21, no. 3, p. 101–107.
Wang, C.Y., and Zhou, M.-F., 2007, Permian flood basalts and mafic intrusions in the Jinping (SW China)–Song Da (northern Vietnam) district: Mantle sources, crustal contamination and sulfide segregation: Chemical Geology, v. 243, p. 317–343.
Watson, E.B., and Harrison, T.M., 2005, Zircon thermometer reveals minimum melting conditions on earliest Earth: Science, v. 308, p. 841.
Watson, E.B., Wark, D.A., and Thomas, J.B., 2006, Crystallization thermometers for zircon and rutile: Contributions to Mineralogy and Petrology, v. 151, p. 413–433.
Weaver, B.L., 1991, The origin of ocean island basalt end–member compositions: Trace element and isotopic constraints: Earth and Planetary Science Letters, v. 104, p. 387–397.
Willbold, M., and Stracke, A., 2006, Trace element composition of mantle end–members, implications for recycling of oceanic and upper and lower continental crust: Geochemistry Geophysics Geosystems, v. 7, no. 4, doi: 10.1029/2005GC001005.
Wilson, M., 1989, Igneous petrogenesis: London, Unwin Hyman, p. 245–285.
Winchester, J.A., and Floyd, P.A., 1977, Geochemical discrimination of different Magma series and their differentiation products using immobile elements: Chemical Geology, v. 20, p. 325–343.
Wood, D.A., 1980, The application of a Th–Hf–Ta diagram to problems of tectonomagmatic classification and to establishing the nature of crustal contamination of basaltsic lavas of the British tertiary volcanic province: Earth and Planetary Science Letters, v. 50, p. 11–30.
Xiao, L., He, Q., Pirajno, F., Ni, P., Du, J., and Wei, Q., 2008, Possible correlation between a mantle plume and the evolution of Paleo–Tethys Jinshajiang ocean: Evidence from a volcanic rifted margin in the Xiaru–Tuoding area, Yunnan, SW China: Lithos, v. 100, p. 112–126.
Xu, Y.G., Chung, S.L., Jahn, B.M., and Wu, G., 2001, Petrologic and geochemical constraints on the petrogenesis of Permian–Triassic Emeishan flood basalts in southwestern China: Lithos, v. 58, p. 145–168.
Xu, Y.-G., He, B., Chung, S.L., Menzies, M.A., and Frey, F.A., 2004, Geologic, geochemical and geophysical consequences of plume involvement in the Emeishan flood–basalt province: Geology, v. 32, p. 917.
Xue, C.D., 2002, The space–time structure model of the Gejiu super large tin–copper–polymetallic deposit [Ph.D. thesis]: China, Kunming University of Science and Technology, 149 p. (in Chinese with English abstract).
YBGMR (Yunnan Bureau of Geology and Mineral Resources), 1982, Regional geology of Yunnan Province: Bejing, Geological Publishing House, 728 p. (in Chinese with English abstract).
Zhang, H.F., Sun, M., Lu, F.X., Zhou, X.M., Zhou, M.F., Liu, Y.S., and Zhang, G.H., 2001, Moderately depleted lithospheric mantle underneath the Yangtze Block: Evidence from a garnet lherzolite xenolith in the Dahongshan kimberlite: Journal of Geochemistry, v. 35, p. 315–331.

Zheng, R.C., and Liu, W.J., 1993, The volcanic rocks and tectonic environments during hercynian–indosinian stage in Ailaos mountain and western Youjiang: Journal of Chengdu Collage of Geology, v. 20, p. 10–23 (in Chinese).

Zhong, H., Campbell, I.H., Zhu, W.-G., Allen, C.M., Hu, R.Z., Xie, L.W., and He, D.F., 2011, Timing and source constraints on the relationship between mafic and felsic intrusions in the Emeishan large igneous province: Geochimica et Cosmochimica Acta, v. 75, p. 1374–1395.

Zhou, M.F., Arndt, N.T., Malpas, J., Wang, C.Y., and Kennedy, A.K., 2008, Two magma series and associated ore deposit types in the Permian Emeishan large igneous province, SW China: Lithos, v. 103, p. 352–368.

Zhou, M.F., Malpas, J., Song, X.Y., Robinson, P.T., Sun, M., Kennedy, A.K., Lesher, C.M., and Keays, R.R., 2002, A temporal link between the Emeishan large igneous province (SW China) and the end–Guadalupian mass extinction: Earth and Planetary Science Letters, v. 196, p. 113–122.

Zindler, A., and Hart, S.R., 1986, Chemical geodynamics: Annual Review of Earth and Planetary Science, v. 14, p. 493–571.

Zong, K.Q., Liu, Y.S., Gao, C.G., Hu, Z.C., Gao, S., and Gong, H.J., 2010, In situ U–Pb dating and trace element analysis of zircons in thin sections of eclogite: Refining constraints on the ultra high-pressure metamorphism of the Sulu terrane, China: Chemical Geology, v. 269, p. 237–251.